THE JOURNAL OF PHYSICAL CHEMISTRY C
A JOURNAL OF THE AMERICAN CHEMICAL SOCIETY

pubs.acs.org/JPCC

Article

# Structure-Dependent Electrical Double-Layer Capacitances of the Basal Plane Pd(*hkl*) Electrodes in $HClO_4$

Elena Gubanova,*[,‖] Thorsten O. Schmidt,[‖] Sebastian Watzele, Vitaly Alexandrov,* and Aliaksandr S. Bandarenka*

Cite This: *J. Phys. Chem. C* 2022, 126, 11414–11420

Read Online

ACCESS | Metrics & More | Article Recommendations | Supporting Information

**ABSTRACT:** Electrical double-layer capacitance ($C_{DL}$) measurements are among the key experiments in physical electrochemistry aimed to understand the properties of electrified solid/liquid interfaces. $C_{DL}$ serves as a critical parameter for developing physical models of electrochemical interfaces. Palladium (Pd) electrodes are among the most widely used functional materials in many applications, including (electro)catalysis. In this work, we report on double-layer capacitances of the basal plane Pd(111), Pd(100), and Pd(110) electrodes in aqueous $HClO_4$ electrolytes measured using electrochemical impedance spectroscopy. Importantly, we find that the $C_{DL}$ values estimated at the minima of the capacitance vs electrode potential curves can be correlated with the density-functional-theory (DFT)-calculated adsorption energies for water molecules and the coordination of electrode surface atoms. Our results thus suggest that it might be possible to find simple descriptors of the electrical double layer (EDL) analogous to those used for functional electrode materials. Taken together, such descriptors could be employed for efficient high-throughput screening of various electrode/electrolyte interfaces, such as in supercapacitor and electrocatalytic systems.

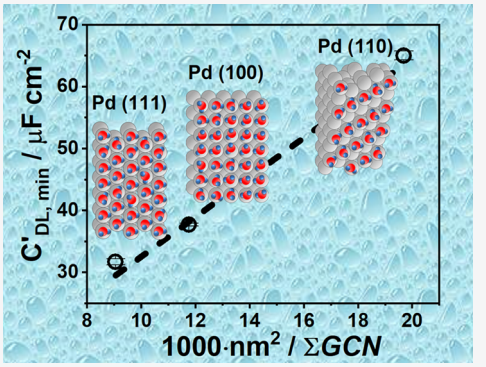


Downloaded via UNIV OF NEBRASKA LINCOLN on August 23, 2022 at 14:40:32 (UTC).
See https://pubs.acs.org/sharingguidelines for options on how to legitimately share published articles.

## INTRODUCTION

The knowledge of basic parameters characterizing the electrified solid/liquid interface is of great importance to understanding its functionality, such as catalytic properties.[1−6] The capacitance of the electrical double layer ($C_{DL}$) is one of those critical parameters.[7] For example, the position of the $C_{DL}$ minima is often associated with the so-called potential of zero charge or maximum entropy, indicating which electrolyte compositions are beneficial for promoting electrocatalytic reactions.[8−14] However, despite their importance, the $C_{DL}$ values of model single-crystal electrodes are available only for a relatively small amount of systems (see, *e.g.*,[15−17]). This can be partly explained by the challenges in preparing single-crystal electrodes and fundamental issues related to the measurements, for example, due to the so-called frequency dispersion of the double-layer capacitance,[18−20] even for flat single-crystal electrodes in electrolytes, which do not contain specifically adsorbing ions.

Palladium(Pd) is a versatile material with a wide range of applications. In electrocatalysis, it is considered among the so-called energy materials, catalyzing the hydrogen evolution, hydrogen oxidation, and oxygen reduction reactions.[21] In this work, we report on the double-layer capacitances of the basal plane Pd(*hkl*) single-crystal electrodes, namely, Pd(111), Pd(100), and Pd(110). The utilized electrolyte is 0.1 M $HClO_4$, a standard medium used in multiple electrocatalytic and other physicochemical applications. Furthermore, we establish the hypothesis on the intrinsic correlations between the energy adsorption characteristics of electrolyte components, the structure of the Pd(*hkl*) surfaces, and the double-layer capacitances found close to the potential of zero charge (PZC). We suggest that these correlations can be used to improve or supplement the rational design of new materials for various energy conversion and storage applications.

## EXPERIMENTAL SECTION

The Pd(111), Pd(100), and Pd(110) disk electrodes (Ø: 5 mm, 99.999%, MaTecK, Jülich, Germany) were oriented more precisely than 0.05° and polished to a nominal roughness of less than 30 nm. Before the cyclic voltammetric (CV) and electrochemical impedance spectroscopy (EIS) experiments, the crystals were annealed for 2 h in an Ar (5.0, Westfalen, Germany) atmosphere at 950 °C in a furnace (Heraeus Instruments RO 7/50, Germany), cooled down overnight, and transferred into a standard three-electrode cell. To avoid an oxidation during the transportation by exposing the sample to the air, the electrode surface was protected by a droplet of

**Received:** May 5, 2022
**Revised:** June 11, 2022
**Published:** July 5, 2022

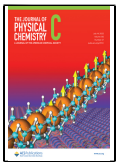

ACS Publications

© 2022 American Chemical Society

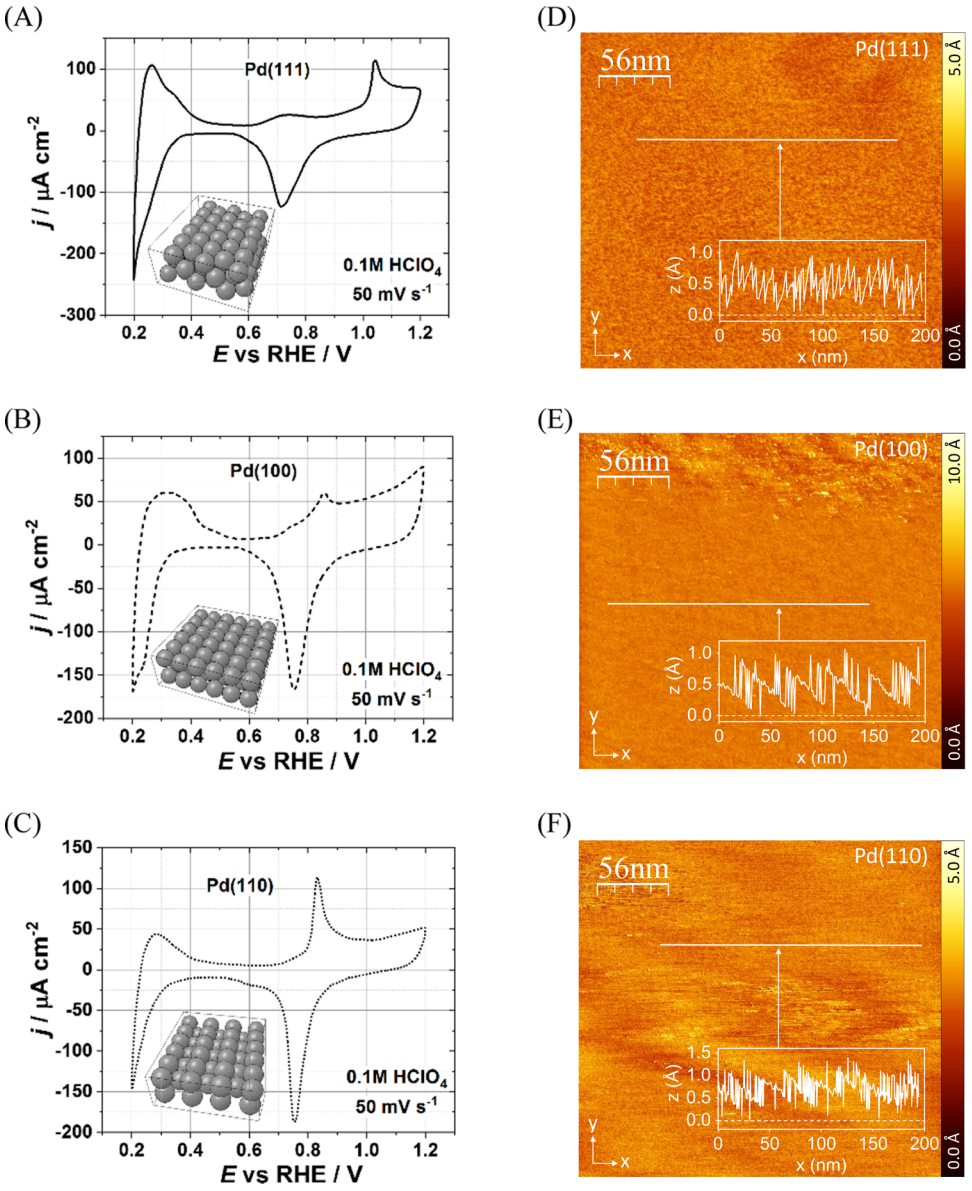


**Figure 1.** (A–C) Typical cyclic voltammograms (first cycles) and (D–F) corresponding EC-STM pictures of freshly annealed (A, D) Pd(111), (B, E) Pd(100), and (C, F) Pd(110) in 0.1 M HClO4. Scanning rate for CVs (A–C): 50 mV $s^{-1}$.

ultrapure water (Evoqua Milli-Q,18.2 MΩ cm). Electrochemical scanning tunneling microscopy (EC-STM) imaging was performed under potential control (0.0 V vs platinum) to prevent electrochemical surface reactions. In all experiments, 0.1 M $HClO_4$ (Suprapur, Merck, Germany) was used as an electrolyte. The measurements were performed using a VSP-300 potentiostat (BioLogic, France).

**Electrochemical Voltammetric and Impedance Measurements.** All glassware and Teflon cell parts were cleaned in a piranha solution, a 1:2 mixture of 30% $H_2O_2$ (Suprapur, Merck, Germany) and 96% $H_2SO_4$ (Suprapur, Merck, Germany), and treated/washed with boiling ultrapure Milli-Q water with a resistivity of 18.2 MΩ·cm before the experiments. The standard three-electrode configuration cell was operated with a mercury-mercurous sulfate electrode (MMS) (SI Analytics, Germany) and Pd wire (Ø 0.25 mm, 99.95%, MaTecK, Germany) as the reference and counter electrode, respectively. A starting potential of 0.57 $V_{RHE}$ was used to avoid possible electrochemical surface processes before the actual measurement started. The quality of the annealed single crystalline surface was verified by cyclic voltammetry (CVs) in Ar-saturated 0.1 M $HClO_4$ at a potential range between 0.2 and 1.2 $V_{RHE}$ and a scan rate of 50 mV $s^{-1}$.

The electrochemical impedance spectroscopy (EIS) measurements were performed within a frequency range between 50 kHz and 1 Hz using a perturbation amplitude of 10 mV. To suppress possible potentiostat- and reference electrode-related artifacts, a shunt capacitor was connected between the reference and a dummy electrode. The dummy electrode was placed close to the Luggin capillary. For the EIS data analysis, the housemade software "EIS Spectrum Analyzer 1.3" was used.[22,23] The quality of the recorded spectra was ensured by a Krammer–Kroenig check.

**Electrochemical Scanning Tunneling Microscopy.** Electrochemical scanning tunneling microscopy (EC-STM) imaging was performed using a Nanoscope III SPM Multimode (Veeco Instruments), connected to a Veeco Nanoscope Universal bipotentiostat and a Nanoscope IIID controller in



https://doi.org/10.1021/acs.jpcc.2c03117
J. Phys. Chem. C 2022, 126, 11414–11420

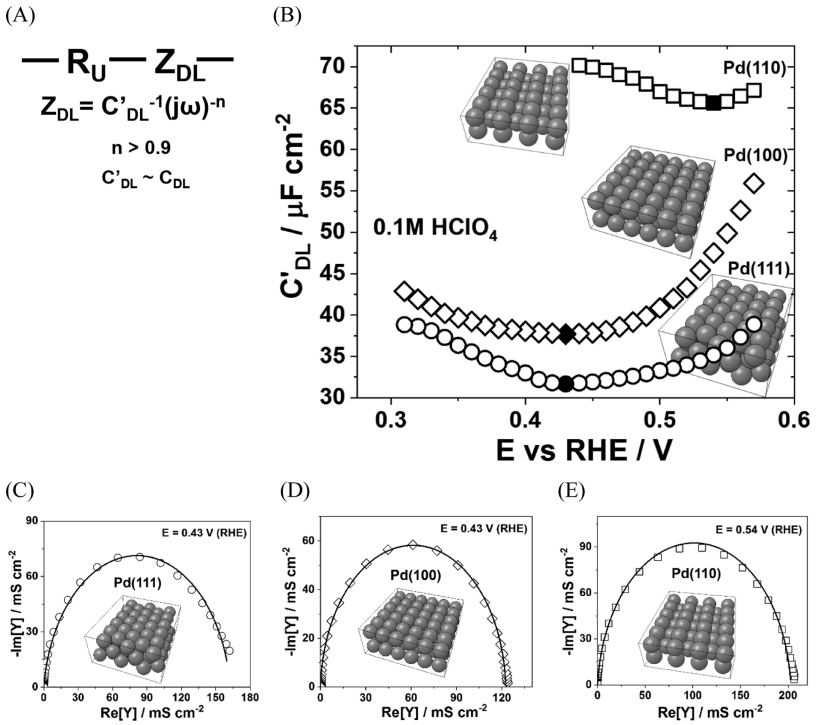


**Figure 2.** Characterization of Pd(*hkl*) electrodes using electrochemical impedance spectroscopy. (A) Equivalent electric circuit. (B) Dependences of the double-layer capacitance on the electrode potential. (C–E) Examples of impedance spectra together with the fitting (solid lines) to the equivalent circuit for the (C) Pd(111), (D) Pd(100), and (E) Pd(110) electrodes.

0.1 M $HClO_4$. For all EC-STM measurements, the single crystals were clamped between a stainless steel plate and a Teflon ring acting as the case of the miniature electrochemical cell. A Pt wire (Ø 0.5 mm, 99.99%, MaTecK, Germany) was used as a quasi-reference electrode and a curled Pd wire (Ø 0.25 mm, 99.95%, MaTecK, Germany) as the counter electrode. The STM-tips were mechanically cut from a Pt/Ir wire (Pt80/Ir20, Ø 0.25, Goodfellow, Germany) and insulated by Apiezon wax. Detailed information on this technique can be found in refs 24–27. The visualization of the EC-STM data was implemented by using WSxM 5.0 Develop 9.4.[28]

**Computational Approach.** The atomic structures of the Pd surfaces with converged computational parameters were taken from the Materials Project[29] and used for adsorption calculations.

*Ab initio* simulations were performed using the density-functional-theory (DFT) plane-wave VASP code.[30−33] The revised Perdew–Burke–Ernzerhof (RPBE) exchange-correlation functional[34] together with the PAW Pd, O, and H potentials[35] was employed. The D3 approach within Grimme's formalism was used to correct for nonlocal van der Waals interactions.[36,37] A cutoff energy of 520 eV was employed in all calculations. The structures were optimized until the total energies and atomic forces were converged to within $10^{-5}$ eV and 0.03 eV/Å, respectively. The (100), (110), and (111) surfaces of Pd were modeled using the periodic slabs consisting of eight, eight, and ten atomic layers, respectively, taken from the Materials Project.[29] The dimensions of the cells employed to estimate the adsorption energies for $H_2O$, H, and OH species were 8.38 × 8.38 Å$^2$, 8.38 × 11.86 Å$^2$, and 8.38 × 8.38 Å$^2$, respectively, with a vacuum gap of at least 13 Å. The Monkhorst–Pack *k*-point mesh of 5 x 5 x 1 was used in all slab calculations. The adsorption energies were computed considering water, proton, and hydroxyl species as adsorbates. All calculations were performed for charge-neutral supercells. The negative adsorption energies correspond to attractive interactions between the adsorbate and the metal surface.

All potentials presented in this work for CV, EIS data, and DFT calculations have been referred to the reversible hydrogen electrode (RHE).

## RESULTS AND DISCUSSION

Figure 1 summarizes the results of voltammetric and EC-STM characterization of the Pd(111), Pd(100), and Pd(110) electrodes. The samples demonstrate typical CV profiles (Figure 1A–C)[38,39] with (i) the underpotential deposition of the hydrogen region between *ca.* 0.2 and 0.5 V, (ii) the double-layer region, and (iii) the region of adsorption of the oxygenated species at the electrode potentials more positive than *ca.* 0.6 V. The corresponding EC-STM images (Figure 1D–F) generally reveal smooth surfaces with atomically flat terraces consisting of thousands of Pd atoms.

Figure 2 shows typical examples of the electrochemical impedance spectroscopy data of the investigated palladium electrodes. The equivalent electric circuit (EEC) shown in Figure 2A was found to adequately describe the impedance response of the systems within the double-layer regions (further analysis details are shown in Figure S1 of the Supporting Information). It consists of two elements: the uncompensated resistance associated with the electrolyte, $R_U$, and the impedance of the electrical double layer, $Z_{DL}$, given by the formula presented in Figure 2A. With the exponent *n* approaching 1, $Z_{DL}$ is close to the impedance of an ideal capacitance. Therefore, the corresponding parameter $C'_{DL}$ is further considered as the double-layer capacitance in this study.

The dependences $C'_{DL}$ vs (*E* The dependence $C'_{DL}$ vs (*E* vs RHE)) for the three freshly annealed Pd(*hkl*) electrodes are



https://doi.org/10.1021/acs.jpcc.2c03117
J. Phys. Chem. C 2022, 126, 11414−11420

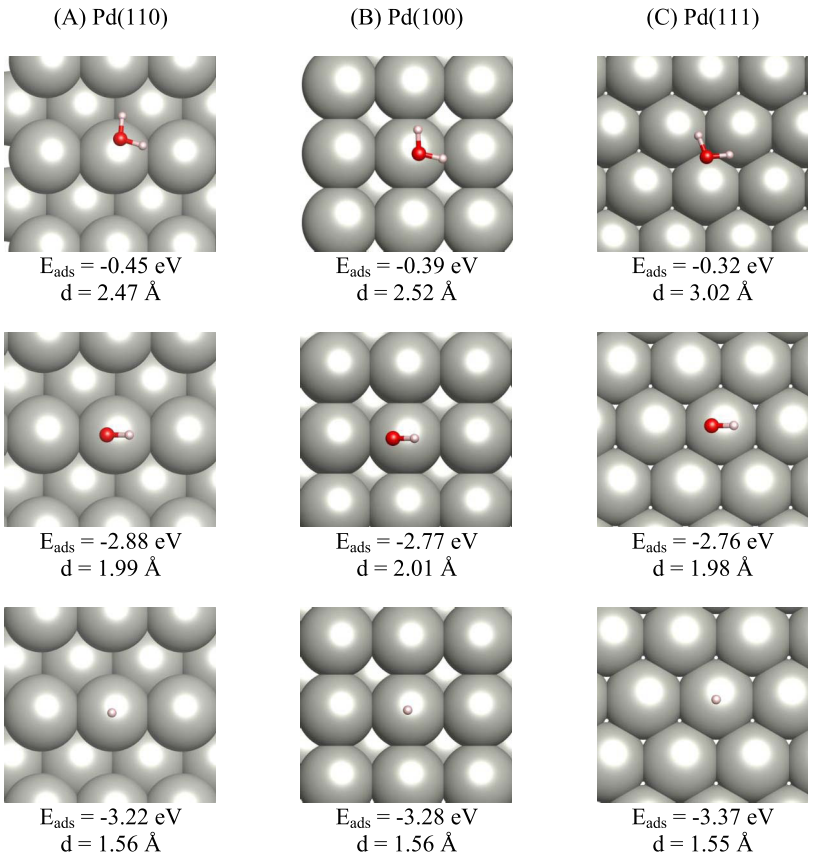


**Figure 3.** (A–C) Adsorbate configurations (top view) and DFT-calculated binding energies for $H_2O$, hydroxyl, and $H^+$ species at Pd(*hkl*) surfaces with the corresponding Pd–O and Pd–H bond lengths indicated in the pictures.

shown in Figure 2B in the potential regions where no significant side electrochemical reactions occur. Typical fitting examples of the admittance spectra to the EEC are shown in Figure 2C–E, confirming that the model describes the experimental data pretty well, with the root-mean-square deviations of less than 2%. It is remarkable in Figure 2B that the double-layer capacitances are drastically different for all three palladium electrodes, considering that they represent examples of very flat model surfaces. In each of the curves in Figure 2B, one can identify the $C'_{DL}$ minima, $C_{DL,min}$, at different electrode potentials and with different corresponding capacitance values. These minima should typically be close to the so-called potentials of zero charges (PZCs), where the net charge of the surface approaches zero.

Somewhat surprisingly, even close to the PZC point, the double-layer capacitances drastically depend on the basal plane surface structure. While classical and recent[40] theories of the double layer do not consider the nature of the electrode and its structure, the experiments show that the electrical double-layer (EDL) capacitance significantly depends not only on the electrolyte composition but also on the electrode structure and its chemical composition.[2,3] Therefore, elucidation of the structure-capacitance relations is an essential part of developing more comprehensive theories of the double layer. As $C_{DL,min}$ also plays a significant role in understanding the electrified interface and the electrocatalytic interfacial charge transfer, in the following, we analyze these data in more detail.

First of all, we hypothesize that $C_{DL,min}$ reflects the intrinsic interactions between the surface and the electrolyte components with minimal influence of the excessive electrode charge. DFT calculations were used to quantify the adsorption energy for the most important strongly interacting species. Three types of species were considered: water molecules, $H^+$, and $OH^-$ species. The results of these calculations are summarized in Figure 3.

It can be seen that $H^+$ species are characterized by the strongest adsorption on the top sites of the Pd surfaces, followed by $OH^-$ and then $H_2O$. Moreover, the corresponding Pd-H and Pd-O bond lengths for the $H^+$ and $OH^-$ adsorbates are almost unaffected by the surface structure (<1%), while for $H_2O$, the bond length is significantly stronger influenced by the surface structure. Therefore, one can assume that the most critical interacting species for the $C_{DL}$ analysis are water molecules. Further, they are likely to significantly impact the overall thickness of the inner Helmholz layer in the double-layer structure. In turn, this should be reflected by variations of the double-layer capacitance for different surfaces.

For the detailed study of this effect, it is essential to parametrize the Pd(*hkl*) structures to correlate structure-related information with the double-layer capacitances. One can do that using the so-called generalized coordination numbers (GCNs).[41−43] GCN is a parameter that can be considered as a simple quantitative measure related to the structure linking it with an electron density function at the surface. Therefore, GCN is a useful descriptor for the affinity of the surface to the electrolyte components. It considers the first and the second nearest neighbors of the accessible adsorption sites and can be calculated using the eq 1, weighting each first-nearest-neighbor atom ($j$) by its conventional coordination number ($cn(j)$)[43]



https://doi.org/10.1021/acs.jpcc.2c03117
J. Phys. Chem. C 2022, 126, 11414−11420

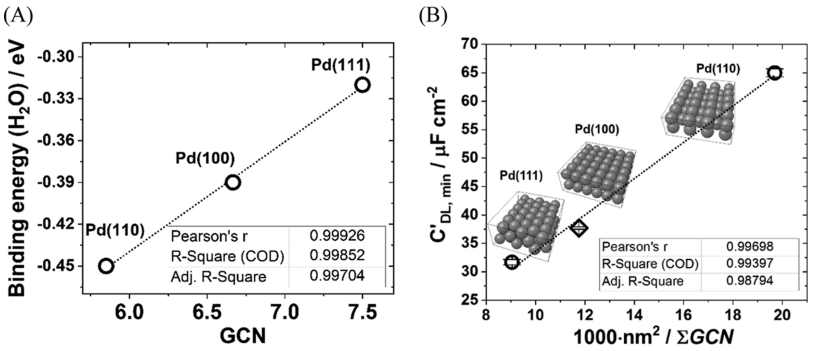


**Figure 4.** (A) DFT-calculated binding energies for $H_2O$ molecules for different Pd(*hkl*) surfaces correlated with the GCNs. (B) Double-layer capacitances found at the minima of the capacitance/electrode potential curves correlated with the $F_e$ parameter defined via surface area normalized generalized coordination numbers.

$$\mathrm{GCN} = (1 + S)^{-1}\left[\sum cn(j)/cn_{\max}\right] \quad (1)$$

where $S$ is the percentage of strain (negative or positive for compressive or tensile strain) and $cn_{max}$ is the maximum number of the direct neighbors in the bulk phase, which is defined as 12 on *fcc* and *hcp* crystals, and as 8 for the *bcc* ones (examples of GCN calculations for the 111, 100, and 110 palladium surfaces are given in the Supporting Information, Figure S2). By assuming zero strain for the freshly annealed surfaces, one can calculate $\mathrm{GCN}(\mathrm{Pd}_{111}) = 7.5$, $\mathrm{GCN}(\mathrm{Pd}_{100}) = 6.6(6)$, and $\mathrm{GCN}(\mathrm{Pd}_{110}) = 5.85$.

Remarkably, the DFT-calculated binding energies for $H_2O$ molecules scale linearly with the GCNs of the investigated palladium planes (Figure 4A), enabling further parametrization of the surfaces in energetic and structural terms simultaneously. In other words, one can use GCNs to characterize and quantify the affinity of the surface toward electrolyte components (in the following, only $H_2O$ is considered) in simple terms.

To correlate the GCN with the $C_{DL,min}$, consider that the generalized coordination number is a measure of "unsaturated surface electron density." One can assume that the higher this value, the lower the densities and the longer the effective distances between the surface atoms and the first layer of water molecules (see, *e.g.*, Figure 3). One should also consider the different numbers of accessible surface sites for the water molecules per unit area, $S$, for different basal surfaces (see Figure S2 in Supporting Information). Therefore, it is reasonable to define a new function, $F_e$, which should be connected to $C_{DL,min}$ in a first approximation

$$F_e = S/\sum \mathrm{GCN} \quad (2)$$

Figure 4B reveals an excellent quasi-linear correlation between $C_{DL,min}$ and $F_e$, where $C_{DL,min}$ increases with decreasing $\sum$GCN, as follows: Pd(111) < Pd(100) < Pd(110).

There must be, of course, not only purely structural reasons, which affect the double-layer capacitances close to the potential of zero charge. For example, one can compare the values for the double-layer capacitances of flat Pd(111) and Pt(111) electrodes at corresponding minima in 0.1 M $HClO_4$ being *ca.* 31.7 μF/cm$^2$ and *ca.* 60 μF/cm$^2$,[44] respectively. This is an indicator that also the chemical nature (*via* dissimilar surface electronic properties) of the electrode is important, and this requires further investigations.

## CONCLUSIONS

In conclusion, we carried out EIS, voltammetric, and electrochemical scanning tunneling microscopy characterizations of the Pd(111), Pd(100), and Pd(110) electrodes. The EIS measurements revealed a strong surface dependence of the double-layer capacitance close to the potential of zero charge, being *ca.* 31.7 μF/cm$^2$ for Pd(111), *ca.* 37.7 μF/cm$^2$ for Pd(100), and *ca.* 65 μF/cm$^2$ for Pd(110). We were also able to correlate the capacitance data with the surface adsorption energies for water species and the generalized coordination numbers of the Pd surfaces. The results of this work thus suggest that it may be possible to characterize the EDL properties such as the double-layer capacitance using simple physical descriptors. Further joint experiment–theory investigations are necessary to generalize the obtained results to other electrochemical systems.

## ASSOCIATED CONTENT

### Supporting Information

The Supporting Information is available free of charge at https://pubs.acs.org/doi/10.1021/acs.jpcc.2c03117.

Estimations related to the generalized coordination numbers. Additional analysis of electrochemical impedance spectroscopy data at the potentials of the $C'_{DL}$ minima (PDF)

## AUTHOR INFORMATION

### Corresponding Authors

**Elena Gubanova** – *Physics of Energy Conversion and Storage, Department of Physics, Technical University of Munich, 85748 Garching bei München, Germany*; Email: elena.gubanova@tum.de

**Vitaly Alexandrov** – *Department of Chemical and Biomolecular Engineering and Nebraska Center for Materials and Nanoscience, University of Nebraska-Lincoln, Lincoln, Nebraska 68588, United States*; orcid.org/0000-0003-2063-6914; Email: valexandrov2@unl.edu

**Aliaksandr S. Bandarenka** – *Physics of Energy Conversion and Storage, Department of Physics, Technical University of Munich, 85748 Garching bei München, Germany; Catalysis Research Center, Technical University of Munich, 85748 Garching bei München, Germany*; orcid.org/0000-0002-5970-4315; Email: bandarenka@ph.tum.de



https://doi.org/10.1021/acs.jpcc.2c03117
J. Phys. Chem. C 2022, 126, 11414–11420

### Authors

**Thorsten O. Schmidt** − *Physics of Energy Conversion and Storage, Department of Physics, Technical University of Munich, 85748 Garching bei München, Germany;* orcid.org/0000-0002-8262-1649

**Sebastian Watzele** − *Physics of Energy Conversion and Storage, Department of Physics, Technical University of Munich, 85748 Garching bei München, Germany*

Complete contact information is available at: https://pubs.acs.org/10.1021/acs.jpcc.2c03117

### Author Contributions

‖E.G. and T.O.S. contributed equally to this work.


### Notes

The authors declare no competing financial interest.

## ■ ACKNOWLEDGMENTS

This project has received funding from the European Union's Horizon 2020 research and innovation program under grant agreement HERMES No 952184. The authors also would like to thank the German Research Foundation (DFG) under Germany's excellence strategy − EXC 2089/1−390776260, Germany's excellence cluster "e-conversion", and the DFG projects BA 5795/5-1 and BA 5795/6-1. They are thankful to Lewin V. Deville (TUM) for his assistance concerning the EC-STM measurements. V.A. acknowledges the National Science Foundation (NSF) support through the NSF CAREER award (grant no. CBET-1941204). This work used the Extreme Science and Engineering Discovery Environment (XSEDE), which is supported by the National Science Foundation grant number ACI-1548562, through allocation TG-CHE170029.

## ■ REFERENCES


(1) Lust, E. Electrical Double Layers. Double Layers at Single-crystal and Polycrystalline Electrodes. In *Encyclopedia of Electrochemistry*, Bard, A. J., Ed.; Wiley, 2002.

(2) Garlyyev, B.; Xue, S.; Watzele, S.; Scieszka, D.; Bandarenka, A. S. Influence of the Nature of the Alkali Metal Cations on the Electrical Double-Layer Capacitance of Model Pt(111) and Au(111) Electrodes. *J. Phys. Chem. Lett.* **2018**, *9*, 1927−1930.

(3) Xue, S.; Garlyyev, B.; Auer, A.; Kunze-Liebhäuser, J.; Bandarenka, A. S. How the Nature of the Alkali Metal Cations Influences the Double-Layer Capacitance of Cu, Au and Pt Single-Crystal Electrodes. *J. Phys. Chem. C* **2020**, *124*, 12442−12447.

(4) Simon, P.; Gogotsi, Y.; Dunn, B. Where Do Batteries End and Supercapacitors Begin? *Science* **2014**, *343*, 1210−1211.

(5) Kornyshev, A. A. Double-Layer in Ionic Liquids: Paradigm Change? *J. Phys. Chem. B* **2007**, *111*, 5545−5557.

(6) Sebastián-Pascual, P.; Shao-Horn, Y.; Escudero-Escribano, M. Toward Understanding the Role of the Electric Double Layer Structure and Electrolyte Effects on Well-Defined Interfaces for Electrocatalysis. *Curr. Opin. Electrochem.* **2022**, *32*, No. 100918.

(7) Haid, R. W.; Ding, X.; Sarpey, T. K.; Bandarenka, A. S.; Garlyyev, B. Exploration of the Electrical Double-Layer Structure: Influence of Electrolyte Components on the Double-Layer Capacitance and Potential of Maximum Entropy. *Curr. Opin. Electrochem.* **2022**, *32*, No. 100882.

(8) Ledezma-Yanez, I.; Wallace, W. D. Z.; Sebastián-Pascual, P.; Climent, V.; Feliu, J. M.; Koper, M. T. M. Interfacial Water Reorganization as a pH-dependent Descriptor of the Hydrogen Evolution Rate on Platinum Electrodes. *Nat. Energy* **2017**, *2*, No. 17031.

(9) Ding, X.; Scieszka, D.; Watzele, S.; Xue, S.; Garlyyev, B.; Haid, R. W.; Bandarenka, A. S. A Systematic Study of the Influence of Electrolyte Ions on the Electrode Activity. *ChemElectroChem* **2022**, *9*, No. e202101088.

(10) Deng, B.; Huang, M.; Zhao, X.; Mou, S.; Dong, F. Interfacial Electrolyte Effects on Electrocatalytic $CO_2$ Reduction. *ACS Catal.* **2022**, *12*, 331−362.

(11) Huang, B.; Rao, R. R.; You, S.; Myint, K. H.; Song, Y.; Wang, Y.; Ding, W.; Giordano, L.; Zhang, Y.; Wang, T.; Muy, S.; Katayama, Y.; Grossman, J. C.; Willard, A. P.; Xu, K.; Jiang, Y.; Shao-Horn, Y. Cation- and pH-Dependent Hydrogen Evolution and Oxidation Reaction Kinetics. *JACS Au* **2021**, *1*, 1674−1687.

(12) Kelly, S. R.; Kirk, Ch.; Chan, K.; Nørskov, J. K. Electric Field Effects in Oxygen Reduction Kinetics: Rationalizing pH Dependence at the Pt(111), Au(111), and Au(100) Electrodes. *J. Phys. Chem. C* **2020**, *124*, 14581−14591.

(13) Kelly, S. R.; Heenen, H. H.; Govindarajan, N.; Chan, K.; Nørskov, J. K. OH Binding Energy as a Universal Descriptor of the Potential of Zero Charge on Transition Metal Surfaces. *J. Phys. Chem. C* **2022**, *126*, 5521−5528.

(14) Li, J.; Stenlid, J. H.; Ludwig, T.; Lamoureux, P. S.; Abild-Pedersen, F. Modeling Potential-Dependent Electrochemical Activation Barriers: Revisiting the Alkaline Hydrogen Evolution Reaction. *J. Am. Chem. Soc.* **2021**, *143*, 19341−19355.

(15) Sadkowski, A.; Mothe, A. J.; Neves, R. S. Characterisation of Au(111) and Au(210)/Aqueous Solution Interfaces by Electrochemical Immittance Spectroscopy. *J. Electroanal. Chem.* **1998**, *455*, 107−119.

(16) Pajkossy, T.; Kolb, D. M. Anion-Adsorption-Related Frequency-Dependent Double Layer Capacitance of the Platinum-Group Metals in the Double Layer Region. *Electrochim. Acta* **2008**, *53*, 7403−7409.

(17) Schouten, K. J. P.; van der Niet, M. J. T. C.; Koper, M. T. M. Impedance Spectroscopy of H and OH Adsorption on Stepped Single-Crystal Platinum Electrodes in Alkaline and Acidic Media. *Phys. Chem. Chem. Phys.* **2010**, *12*, 15217−15224.

(18) Lasia, A. The Origin of the Constant Phase Element. *J. Phys. Chem. Lett.* **2022**, *13*, 580−589.

(19) Bandarenka, A. S. Exploring the Interfaces Between Metal Electrodes and Aqueous Electrolytes with Electrochemical Impedance Spectroscopy. *Analyst* **2013**, *138*, 5540−5554.

(20) Tymoczko, J.; Colic, V.; Bandarenka, A. S.; Schuhmann, W. Detection of 2D Phase Transitions at the Electrode/Electrolyte Interface Using Electrochemical Impedance Spectroscopy. *Surf. Sci.* **2015**, *631*, 81−87.

(21) Kucernak, A. R. J.; Fahy, K. F.; Naranammalpuram Sundaram, V. N. Facile Synthesis of Palladium Phosphide Electrocatalysts and Their Activity for the Hydrogen Oxidation, Hydrogen Evolutions, Oxygen Reduction and Formic Acid Oxidation Reactions. *Catal. Today* **2016**, *262*, 48−56.

(22) Bondarenko, A. S. Analysis of Large Experimental Datasets in Electrochemical Impedance Spectroscopy. *Anal. Chim. Acta* **2012**, *743*, 41−50.

(23) Bandarenka, A. S. Development of Hybrid Algorithms for EIS Data Fitting, a book chapter. In *Lecture Notes on Impedance Spectroscopy. Measurement, Modeling and Applications*, Kanoun, O., Ed.; CRC Press, Tailor and Francis Group: London, 2013; Vol. *4*, pp 29−36.

(24) Binnig, G.; Rohrer, H. Scanning Tunneling Microscopy - from Birth to Adolescence. *Rev. Mod. Phys.* **1987**, *59*, 615−625.

(25) Pfisterer, J. H. K.; Liang, Y.; Schneider, O.; Bandarenka, A. S. Direct Instrumental Identification of Catalytically Active Surface Sites. *Nature* **2017**, *549*, 74−77.

(26) Haid, R. W.; Kluge, R. M.; Liang, Y.; Bandarenka, A. S. In Situ Quantification of the Local Electrocatalytic Activity via Electrochemical Scanning Tunneling Microscopy. *Small Methods* **2021**, *5*, No. 2000710.

(27) Haid, R. W.; Kluge, R. M.; Schmidt, T. O.; Bandarenka, A. S. In-situ Detection of Active Sites for Carbon-based Bifunctional Oxygen Reduction and Evolution Catalysis. *Electrochim. Acta* **2021**, *382*, No. 138285.

(28) Horcas, I.; Fernández, R.; Gomez-Rodriguez, J.; Colchero, J.; Gómez-Herrero, J.; Baro, A. WSXM: A Software for Scanning Probe Microscopy and a Tool for Nanotechnology. *Rev. Sci. Instrum.* **2007**, *78*, No. 013705.
(29) Jain, A.; Ong, S. P.; Hautier, G.; Chen, W.; Richards, W. D.; Dacek, S.; Cholia, S.; Gunter, D.; Skinner, D.; Ceder, G.; Persson, K. A. The Materials Project: A Materials Genome Approach to Accelerating Materials Innovation. *APL Mater.* **2013**, *1*, No. 011002.
(30) Kresse, G.; Hafner, J. Ab Initio Molecular Dynamics For Liquid Metals. *Phys. Rev. B Condens Matter.* **1993**, *47*, 558−561.
(31) Kresse, G.; Hafner, J. Ab Initio Molecular-Dynamics Simulation of the Liquid-Metal-Amorphous-Semiconductor Transition in Germanium. *Phys. Rev. B Condens Matter.* **1994**, *49*, 14251−14269.
(32) Kresse, G.; Furthmuller, J. Efficiency of Ab-initio Total Energy Calculations for Metals and Semiconductors Using a Plane-Wave Basis Set. *Comput. Mater. Sci.* **1996**, *6*, 15−50.
(33) Kresse, G.; Furthmüller, J. Efficient Iterative Schemes for ab Initio Total-Energy Calculations Using a Plane-Wave Basis Set. *Phys. Rev. B Condens Matter.* **1996**, *54*, 11169−11186.
(34) Hammer, B.; Hansen, L. B.; Nørskov, J. K. Improved Adsorption Anergetics within Density-Functional Theory Using Revised Perdew-Burke-Ernzerhof Functionals. *Phys. Rev. B* **1999**, *59*, 7413−7421.
(35) Blöchl, P. E. Projector Augmented-Wave Method. *Phys. Rev. B Condens Matter.* **1994**, *50*, 17953−17979.
(36) Grimme, S. Semiempirical GGA-Type Density Functional Constructed with a Long-Range Dispersion Correction. *J. Comput. Chem.* **2006**, *27*, 1787−1799.
(37) Grimme, S.; Antony, J.; Ehrlich, S.; Krieg, S. A Consistent and Accurate Ab Initio Parametrization of Density Functional Dispersion Correction (DFT-D) for the 94 elements H-Pu. *J. Chem. Phys.* **2010**, *132*, No. 154104.
(38) Naito, K.; Nakamura, M.; Sakata, O.; Hoshi, N. Surface X-ray Scattering of Pd(111) and Pd(100) Electrodes during the Oxygen Reduction Reaction. *Electrochemistry* **2011**, *79*, 256−260.
(39) Hoshi, N.; Noma, M.; Suzuki, T.; Hori, Y. Structural Effect on the Rate of $CO_2$ Reduction on Single Crystal Electrodes of Palladium. *J. Electroanal. Chem.* **1997**, *421*, 15−18.
(40) Ojha, K.; Doblhoff-Dier, K.; Koper, M. T. M. Double-layer structure of the Pt(111)−aqueous electrolyte interface. *Proc. Nat. Acad. Sci. U.S.A.* **2022**, *119*, No. e2116016119.
(41) Calle-Vallejo, F.; Martínez, J. I.; García-Lastra, J. M.; Sautet, P.; Loffreda, D. Fast Prediction of Adsorption Properties for Platinum Nanocatalysts with Generalized Coordination Numbers. *Angew. Chem., Int. Ed.* **2014**, *53*, 8316−8319.
(42) Calle-Vallejo, F.; Tymoczko, J.; Colic, V.; Vu, Q. H.; Pohl, M. D.; Morgenstern, K.; Loffreda, D.; Sautet, P.; Schuhmann, W.; Bandarenka, A. S. Finding Optimal Surface Sites on Heterogeneous Catalysts by Counting Nearest Neighbors. *Science* **2015**, *350*, 185−189.
(43) Calle-Vallejo, F.; Bandarenka, A. S. Enabling Generalized Coordination Numbers to Describe Strain Effects. *ChemSusChem* **2018**, *11*, 1824−1828.
(44) Bondarenko, A. S.; Stephens, I. E. L.; Bech, L.; Chorkendorff, I. Probing adsorption phenomena on a single crystal Pt-alloy surface under oxygen reduction reaction conditions. *Electrochim. Acta* **2012**, *82*, 517−523.

## Recommended by ACS

**Future Directions for Electrochemical Capacitors**
Liyuan Liu, Patrice Simon, *et al.*
NOVEMBER 11, 2021
ACS ENERGY LETTERS
READ

**Modeling Electrified Pt(111)-$H_{ad}$/Water Interfaces from Ab Initio Molecular Dynamics**
Jia-Bo Le, Jun Cheng, *et al.*
APRIL 06, 2021
JACS AU
READ

**Three-Dimensional Molecular Mapping of Ionic Liquids at Electrified Interfaces**
Shan Zhou, Yingjie Zhang, *et al.*
NOVEMBER 23, 2020
ACS NANO
READ

**Charge Storage Mechanisms of Single-Layer Graphene in Ionic Liquid**
Jianglin Ye, Patrice Simon, *et al.*
OCTOBER 05, 2019
JOURNAL OF THE AMERICAN CHEMICAL SOCIETY
READ

Get More Suggestions >



https://doi.org/10.1021/acs.jpcc.2c03117
J. Phys. Chem. C 2022, 126, 11414−11420